CHINESE OPTICS LETTERS

Vol. 21, No. 2 | February 2023

Full description of dipole orientation in organic light-emitting diodes

Lingjie Fan (范灵杰)[1,2], Maoxiong Zhao (赵茂雄)[1,2], Jiao Chu (楚 娇)[1], Tangyao Shen (沈唐尧)[1,2], Minjia Zheng (郑敏嘉)[1], Fang Guan (关 放)[3], Haiwei Yin (殷海玮)[2], Lei Shi (石 磊)[1,2,3,4*], and Jian Zi (资 剑)[1,2,3,4**]

[1] Department of Physics, Key Laboratory of Micro- and Nano-Photonic Structures (Ministry of Education), and State Key Laboratory of Surface Physics, Fudan University, Shanghai 200433, China

[2] Shanghai Engineering Research Center of Optical Metrology for Nano-fabrication (SERCOM), Shanghai 200433, China

[3] Institute for Nanoelectronic Devices and Quantum Computing, Fudan University, Shanghai 200438, China

[4] Collaborative Innovation Center of Advanced Microstructures, Nanjing University, Nanjing 210093, China

*Corresponding author: lshi@fudan.edu.cn

**Corresponding author: jzi@fudan.edu.cn

Received May 25, 2022 | Accepted August 15, 2022 | Posted Online September 20, 2022

Considerable progress has been made in organic light-emitting diodes (OLEDs) to achieve high external quantum efficiency, among which dipole orientation has a remarkable effect. In most cases, the radiation of the dipoles in OLEDs is theoretically predicted with only one orientation parameter to match with corresponding experiments. Here, we develop a new theory with three orientation parameters to fully describe the relationship between dipole orientation and power density. Furthermore, we design an optimal test structure for measuring all three orientation parameters. All three orientation parameters could be retrieved from non-polarized spectra. Our theory provides a universal plot of dipole orientations in OLEDs, paving the way for designing more complicated OLED devices.

Keywords: organic light-emitting diodes; dipole orientation; Fourier series expansion.

DOI: 10.3788/COL202321.022601

1. Introduction

Since the first reports of organic light-emitting diodes (OLEDs) in 1987[1], their efficiency has been improved through finding novel phosphorescent materials[2–10], optimizing the thickness of each layer in OLEDs[11–13], etc. In recent years, dipole orientation has also been drawing significant attention for enhancing light extraction from OLEDs[14–21].

The theory of dipole radiation in OLEDs originated from applying the theory of electrical dipoles near an interface to the problem of molecules fluorescing near a surface[22–29]. Related researches have been proposed to enhance the external quantum efficiency[30], in which the theory of the dipole orientation is developed. In previous theories, dipoles in OLEDs are decomposed into vertical dipoles and horizontal dipoles. Then, the power radiated from OLEDs is formed by weighting the power radiated by vertical dipoles and horizontal dipoles in a proportion. The weight, the ratio of vertical dipoles, can be regarded as a parameter describing the vertical orientations of the dipoles in OLEDs.

Recently, along with the OLED manufacturing progress increasingly, it is pointed out that a possible research direction of OLEDs in the future is to take advantage of the dipoles with non-uniform horizontal orientations[31,32]. Some studies point out that the carrier mobility in films using the dipoles perfectly aligning in one direction is much higher than that of films using the dipoles with uniform orientations[33,34]. At the same time, other researchers show that OLEDs with dipoles aligning in one direction can achieve the emission of linearly-polarized light. Then, the application of OLEDs directly emitting orthogonal circularly-polarized light could be realized by letting the linearly-polarized light pass through a quarter-wave plate formed by the liquid crystal[35]. Therefore, the non-uniform horizontal dipole orientation is of great significance for external quantum efficiency, as well as polarization. However, previous works have so far only considered the dipoles in OLEDs with non-uniform vertical orientations and lack of the description of the horizontal component.

Here, we develop a theory that fully describes the dipole orientation and its relationship with power density. Compared with the previous theory, we start from a dipole and consider an orientation distribution function, expressed as a Fourier series, to extend the power density of a dipole to the power density of the dipoles in OLEDs. Theoretically, it is the first time, to the best of

our knowledge, to strictly prove that only three orientation parameters are needed to fully describe the effect of dipole orientation on the power density and extend previous orientation parameters. Two parameters describe the ratios of the x component and z component of the dipoles. One parameter describes the coupling effect between the x component and z component of the dipoles. Finally, by using optical simulation, we design an optimal structure for extracting these three orientation parameters and present different spectra corresponding to different orientation parameters for the test structure. Then, we extract the orientation parameters for the designed optimal structure and compare them with the ground truth to verify our orientation theory.

2. Methods

2.1. Power density of a dipole in OLEDs

For the multi-layer model shown in Fig. 1(a), the emitting layer with refractive index n_0 and thickness h_0 is located between two stacks of layers. These layers have refractive indices $n_{1\pm}, n_{2\pm}, \ldots$ and thicknesses $h_{1\pm}, h_{2\pm}, \ldots$. The upper and lower half-infinite spaces are labeled as ±. The dipoles are located in the middle of layer 0 with a distance $h_{0\pm}$ from the interface at the ± side of the layers. OLEDs, therefore, can be simplified to multi-layer films. Energy reflection and transmission coefficients of multi-layer films are given by

$$\begin{aligned} R_{\pm}^{s,p} &= |r_{\pm}^{s,p}|^2 && \text{for all cases,} \\ T_{\pm}^{s} &= |t_{\pm}^{s}|^2 \frac{k_{z,\pm}}{|k_{z,0}|} && \text{for } \mathrm{Im}(k_{z,\pm}) = 0, \\ T_{\pm}^{p} &= |t_{\pm}^{p}|^2 \frac{n_0^2}{n_{\pm}^2} \frac{k_{z,\pm}}{|k_{z,0}|} && \text{for } \mathrm{Im}(k_{z,\pm}) = 0, \\ T_{\pm}^{s,p} &= 0 && \text{for } \mathrm{Im}(k_{z,\pm}) \neq 0. \end{aligned} \tag{1}$$

$r_{\pm}^{s,p}, t_{\pm}^{s,p}$ are Fresnel reflection and transmission coefficients, as shown in Fig. 1(b), which could be calculated through recursive matrix algorithms[36,37]. These coefficients with subscripts ± represent the reflection and transmission coefficients from the emitting layer (layer 0) to the ± half-infinite space. $k_{\parallel}$ and $k_{z,\pm}$ are the horizontal and z component of the wave vector $k_{\pm}$ in the ± half-infinite space. With the use of the superposition of plane waves, the power $W_{\pm}$ radiated to the half-infinite space ± can be written as an integral:

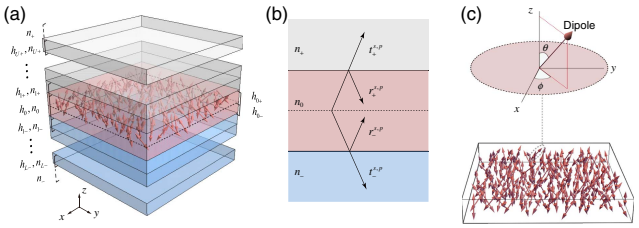

Fig. 1. (a) Multi-layer films for modeling OLEDs. (b) Energy reflection and transmission coefficients of multi-layer films. (c) Upper panel: the orientation of a dipole. Lower panel: dipole orientations in layer 0.

$$W_{\pm} = \int_0^{+\infty} K_{\pm} \mathrm{d}k_{\parallel}^2, \tag{2}$$

where $K_{\pm}$ is the power density of a dipole per unit $\mathrm{d}k_{\parallel}^2$. Based on the polarity, the power density $K_{\pm}$ can be separated into s-polarized power density $K_{\pm}^{s}$ and p-polarized power density $K_{\pm}^{p}$:

$$K_{\pm} = K_{\pm}^{s} + K_{\pm}^{p}. \tag{3}$$

For an electric dipole in the emitting layer with orientation (θ, ϕ), as shown in Fig. 1(c) upper panel, the s-polarized and p-polarized power densities radiated to the ± half-infinite space in the x–z plane per unit $\mathrm{d}k_{\parallel}^2$ have an angular dependence and are related to its dipole orientation[26,28]:

$$\begin{aligned} K_{\pm}^{s} =& \frac{3}{8} \frac{1}{k_0 k_{z,0}} \frac{|1 + r_{\mp}^{s} \exp(2jk_{z,0}h_{0\mp})|^2}{|1 - r_{+}^{s} r_{-}^{s} \exp(2jk_{z,0}h_0)|^2} T_{\pm}^{s} \sin^2(\theta) \sin^2(\phi), \\ K_{\pm}^{p} =& \frac{3}{8} \frac{k_{\parallel}^2}{k_0^3 k_{z,0}} \frac{|1 + r_{\mp}^{p} \exp(2jk_{z,0}h_{0\mp})|^2}{|1 - r_{+}^{p} r_{-}^{p} \exp(2jk_{z,0}h_0)|^2} T_{\pm}^{p} \cos^2(\theta) \\ &+ \frac{3}{8} \frac{k_{z,0}}{k_0^3} \frac{|1 - r_{\mp}^{p} \exp(2jk_{z,0}h_{0\mp})|^2}{|1 - r_{+}^{p} r_{-}^{p} \exp(2jk_{z,0}h_0)|^2} T_{\pm}^{p} \sin^2(\theta) \cos^2(\phi) \\ &- \frac{3}{8} \frac{k_{\parallel}}{k_0^3} \frac{1}{|1 - r_{+}^{p} r_{-}^{p} \exp(2jk_{z,0}h_0)|^2} T_{\mp}^{p} T_{\pm}^{p} \sin(2\theta) \cos(\phi). \end{aligned} \tag{4}$$

For an emission angle α, the angle between the z axis and the detector (observer) in the ± half-infinite space, the power density $K_{\pm}$ per unit $\mathrm{d}k_{\parallel}^2$ can be transformed to the power density $P_{\pm}$ per solid angle, given by

$$P_{\pm} = \frac{k_{\pm}^2 \cos(\alpha)}{\pi} K_{\pm}. \tag{5}$$

2.2. Power density of the dipoles in OLEDs

For dipole orientations in OLEDs shown in Fig. 1(c) lower panel, we can use an orientation distribution function $F(\theta, \phi)$ to describe them. Multiplied with the orientation distribution function and then integrated over the sphere with the polar angle θ and azimuth angle ϕ, the power density of a dipole $P_{\pm}$ can be used to describe the dipoles in OLEDs:

$$\tilde{P}_{\pm} = \int_0^{2\pi} \mathrm{d}\phi \int_0^{\pi} \mathrm{d}\theta P_{\pm} \times F(\theta, \phi), \tag{6}$$

where $\tilde{P}_{\pm}$ is the power density of the dipoles in OLEDs, related to the emission angle α and the dipole orientations.

By using the Fourier series expansion, the orientation distribution function $F(\theta, \phi)$ could be expanded into the Fourier series:

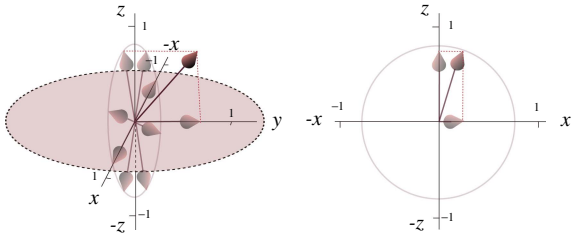

Fig. 2. Physical meaning of the orientation parameters v_x, v_z, and $v_{x,z}$. Left panel: the dipole vector is decomposed along the y axis and x–z plane. Right panel: the dipole vector in the x–z plane is further decomposed along the x and z axes.

$$F(\theta,\phi)=\sum_{l,m=1}^{\infty}\lambda_{l,m}[a_{l,m}\cos(2l\theta)\cos(m\phi)+b_{l,m}\cos(2l\theta)\sin(m\phi)+c_{l,m}\sin(2l\theta)\cos(m\phi)+d_{l,m}\sin(2l\theta)\sin(m\phi)], \tag{7}$$

with

$$\begin{aligned}&\lambda_{l,m}=\tfrac{1}{4}\quad \text{for } l=0,\ m=0,\\ &\lambda_{l,m}=\tfrac{1}{2}\quad \text{for } l=0,\ m\neq 0 \text{ or } l\neq 0,\ m=0,\\ &\lambda_{l,m}=1\quad \text{for } l\neq 0,\ m\neq 0.\end{aligned} \tag{8}$$

Coefficients $a_{l,m}$, $b_{l,m}$, $c_{l,m}$, and $d_{l,m}$ are given by

$$\begin{aligned}a_{l,m}&=\frac{2}{\pi^2}\int_0^{2\pi}\int_0^{\pi}F(\theta,\phi)\cos(2l\theta)\cos(m\phi)\mathrm{d}\theta\mathrm{d}\phi,\\ b_{l,m}&=\frac{2}{\pi^2}\int_0^{2\pi}\int_0^{\pi}F(\theta,\phi)\cos(2l\theta)\sin(m\phi)\mathrm{d}\theta\mathrm{d}\phi,\\ c_{l,m}&=\frac{2}{\pi^2}\int_0^{2\pi}\int_0^{\pi}F(\theta,\phi)\sin(2l\theta)\cos(m\phi)\mathrm{d}\theta\mathrm{d}\phi,\\ d_{l,m}&=\frac{2}{\pi^2}\int_0^{2\pi}\int_0^{\pi}F(\theta,\phi)\sin(2l\theta)\sin(m\phi)\mathrm{d}\theta\mathrm{d}\phi.\end{aligned} \tag{9}$$

Then, the orientation distribution function in the form of the Fourier series is substituted into Eq. (6). Due to the angular dependence relation of the power density of a dipole, as shown in Eq. (4), and also because the integral values of the product of two orthogonal trigonometric functions are all zero, only four Fourier components and coefficients are left among these integrations of the Fourier series. The orientation distribution function can be simplified to the orientation distribution function with four Fourier coefficients, given by

$$F(\theta,\phi)=\frac{1}{2\pi^2}+\frac{1}{2}a_{1,0}\cos(2\theta)+\frac{1}{2}a_{0,2}\cos(2\phi)+c_{1,1}\sin(2\theta)\cos(\phi)+a_{1,2}\cos(2\theta)\cos(2\phi). \tag{10}$$

The power density per solid angle of the dipoles in OLEDs, for an emission angle α in the ± half-infinite space, can be written in the form of Fourier coefficients $a_{1,0}$, $a_{0,2}$, $c_{1,1}$, and $a_{1,2}$, and different components of the power density $\widetilde{\mathcal{P}}_{\pm}^{s}$, $\widetilde{\mathcal{P}}_{\pm}^{p1}$, $\widetilde{\mathcal{P}}_{\pm}^{p2}$, and $\widetilde{\mathcal{P}}_{\pm}^{p3}$:

$$\begin{aligned}\tilde{P}_{\pm}=&\widetilde{\mathcal{P}}_{\pm}^{s}\times\frac{\pi^2}{8}\left(\frac{2}{\pi^2}-a_{1,0}-(a_{0,2}-a_{1,2})\right)\\ &+\widetilde{\mathcal{P}}_{\pm}^{p1}\times\frac{\pi^2}{4}\left(\frac{2}{\pi^2}+a_{1,0}\right)\\ &+\widetilde{\mathcal{P}}_{\pm}^{p2}\times\frac{\pi^2}{8}\left(\frac{2}{\pi^2}-a_{1,0}+(a_{0,2}-a_{1,2})\right)\\ &+\widetilde{\mathcal{P}}_{\pm}^{p3}\times\frac{\pi^2}{2}c_{1,1},\end{aligned} \tag{11}$$

with

$$\begin{aligned}\widetilde{\mathcal{P}}_{\pm}^{s}&=\frac{k_{\pm}^2\cos(\alpha)}{\pi}\times\frac{3}{8}\frac{1}{k_0k_{z,0}}\frac{|1+r_{\mp}^{s}\exp(2jk_{z,0}h_{0\mp})|^2}{|1-r_{+}^{s}r_{-}^{s}\exp(2jk_{z,0}h_0)|^2}T_{\pm}^{s},\\ \widetilde{\mathcal{P}}_{\pm}^{p1}&=\frac{k_{\pm}^2\cos(\alpha)}{\pi}\times\frac{3}{8}\frac{k_{\parallel}^2}{k_0^3k_{z,0}}\frac{|1+r_{\mp}^{p}\exp(2jk_{z,0}h_{0\mp})|^2}{|1-r_{+}^{p}r_{-}^{p}\exp(2jk_{z,0}h_0)|^2}T_{\pm}^{p},\\ \widetilde{\mathcal{P}}_{\pm}^{p2}&=\frac{k_{\pm}^2\cos(\alpha)}{\pi}\times\frac{3}{8}\frac{k_{z,0}}{k_0^3}\frac{|1-r_{\mp}^{p}\exp(2jk_{z,0}h_{0\mp})|^2}{|1-r_{+}^{p}r_{-}^{p}\exp(2jk_{z,0}h_0)|^2}T_{\pm}^{p},\\ \widetilde{\mathcal{P}}_{\pm}^{p3}&=-\frac{k_{\pm}^2\cos(\alpha)}{\pi}\times\frac{3}{8}\frac{k_{\parallel}}{k_0^3}\frac{1}{|1-r_{+}^{p}r_{-}^{p}\exp(2jk_{z,0}h_0)|^2}T_{\mp}^{p}T_{\pm}^{p}.\end{aligned} \tag{12}$$

3. Results

3.1. Orientation parameters

The power density $\tilde{P}_{\pm}$ in Eq. (11) is adjusted by three independent parameters $a_{1,0}$, $a_{0,2}-a_{1,2}$, $c_{1,1}$, indicating that only three orientation parameters are needed for a full description of dipole orientations in OLEDs. Therefore, three orientation parameters should be defined based on four Fourier coefficients $a_{1,0}$, $a_{0,2}$, $a_{1,2}$, and $c_{1,1}$.

Here, we define the orientation parameters v_x, v_z, and $v_{x,z}$, where v_x represents the ratio of the x component of the emitting dipoles, v_z represents the ratio of the z component of the emitting dipoles, and $v_{x,z}$ represents the coupling effect between the x component and z component of the emitting dipoles, given by

$$\begin{aligned}v_x&=\frac{\pi^2}{8}\left(\frac{2}{\pi^2}-a_{1,0}+(a_{0,2}-a_{1,2})\right),\\ v_z&=\frac{\pi^2}{4}\left(\frac{2}{\pi^2}+a_{1,0}\right),\\ v_{x,z}&=\frac{\pi^2}{2}c_{1,1}.\end{aligned} \tag{13}$$

Thus, the power density of the dipoles in OLEDs could be written in a form of orientation parameters v_x, v_z, and $v_{x,z}$, and different components of the power density $\widetilde{\mathcal{P}}_{\pm}^{s}$, $\widetilde{\mathcal{P}}_{\pm}^{p1}$, $\widetilde{\mathcal{P}}_{\pm}^{p2}$, and $\widetilde{\mathcal{P}}_{\pm}^{p3}$:

$$\tilde{P}_{\pm}=\widetilde{\mathcal{P}}_{\pm}^{s}\times(1-v_x-v_z)+\widetilde{\mathcal{P}}_{\pm}^{p1}\times v_z+\widetilde{\mathcal{P}}_{\pm}^{p2}\times v_x+\widetilde{\mathcal{P}}_{\pm}^{p3}\times v_{x,z}, \tag{14}$$

where $1 - v_x - v_z$ represents the ratio of the y component of the emitting dipoles.

In the case that there are N possible dipole orientations in OLEDs represented by (θ_i, ϕ_i) and the corresponding dipole vectors are $\mathbf{v_i}$, the orientation distribution function reads

$$F(\theta,\phi) = \frac{1}{N} \times \sum_{i=1}^{N} \delta(\mathbf{v} - \mathbf{v_i}) \sin(\theta) = \frac{1}{N} \times \sum_{i=1}^{N} \delta(\theta - \theta_i)\delta(\phi - \phi_i). \quad (15)$$

Considering Eqs. (13) and (9), the orientation parameters v_x, v_z, $v_{x,z}$ of N dipoles could be obtained:

$$v_x = \frac{1}{N} \sum_{i=1}^{N} \sin^2(\theta_i)\cos^2(\phi_i),$$
$$v_z = \frac{1}{N} \sum_{i=1}^{N} \cos^2(\theta_i),$$
$$v_{x,z} = \frac{1}{N} \sum_{i=1}^{N} \sin(2\theta_i)\cos(\phi_i). \quad (16)$$

Equation (16) verifies the physical meaning of the orientation parameters v_x, v_z, and $v_{x,z}$. As shown in Figs. 1(c) and 2, dipoles are decomposed along the x, y, and z axes. $\sin(\theta)\cos(\phi) \times \sin(\theta)\cos(\phi)$ represents the ratio of the x component of the emitting dipoles, ranging from 0 to 1, $\cos(\theta)\cos(\theta)$ represents the ratio of the z component of the emitting dipoles, ranging from 0 to 1, and $\sin(\theta)\cos(\phi)\cos(\theta)$ represents the coupling effect between the x component and z component of the emitting dipoles ranging from −1 to 1. Also, Eq. (16) provides a simple form for calculating the orientation parameters.

3.2. Structure design

To extract the orientation parameters of the dipoles in OLEDs[38,39], non-polarized spectra should be used, and different components of the power density $\widetilde{\mathcal{P}}_{\pm}^{s}$, $\widetilde{\mathcal{P}}_{\pm}^{p1}$, $\widetilde{\mathcal{P}}_{\pm}^{p2}$, and $\widetilde{\mathcal{P}}_{\pm}^{p3}$ are supposed to be adjusted in different shapes but in the same order of magnitude, as suggested by Eq. (14). Therefore, an optimal test structure should be carefully designed for extracting the orientation parameters v_x, v_z, and $v_{x,z}$. We consider a test structure, as shown in Fig. 3 (left panel). An organic thin film is evaporated on the glass substrate, whose thickness is h_0. (h_0 should be chosen for adjusting different components of the power density.) The dipoles are doped in the middle of the emitting layer. The refractive indices of the glass substrate and organic thin film are 1.524 and 1.72, respectively, and the emission wavelength is 500 nm. By using a hemispherical prism along the glass substrate side and measuring the power density radiated into the glass substrate at different angles, the intensity changing with respect to the emission angle could be obtained[21]. Then, the intensity of the spectra at normal direction (0 deg) is normalized to one.

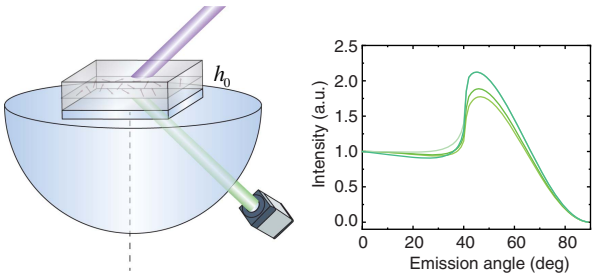

Fig. 3. Test structure designed for extracting the orientation parameters (left panel). The refractive indices of the glass substrate and organic thin film are 1.524 and 1.72, and the emission wavelength is 500 nm. A hemispherical prism, whose refractive index is the same as the substrate, is along the glass substrate side. Simulated non-polarized power densities of the test structure (h_0 = 20 nm) with different orientations (right panel).

Without selecting the appropriate thickness of the organic layer, the spectra with different orientations only have a slight difference, as shown in Fig. 3 (right panel)[40]. It is hard to extract all of the orientation parameters from them.

By adjusting the thickness of organic thin film h_0, different components of the power density $\widetilde{\mathcal{P}}_{\pm}^{s}$, $\widetilde{\mathcal{P}}_{\pm}^{p1}$, $\widetilde{\mathcal{P}}_{\pm}^{p2}$, and $\widetilde{\mathcal{P}}_{\pm}^{p3}$ could be balanced in the same order of magnitude but in different shapes with the help of the interference effect of the micro-cavity, as shown in Fig. 4. When the thickness of organic layer h_0 is near 160 nm, all four components have a significant impact on the power density $\tilde{P}_{\pm}$, compared with the component $\widetilde{\mathcal{P}}_{\pm}^{s}$ being much stronger than others when thickness $h_0 = 20$ nm. Note that extracting orientation parameters of the structure with $h_0 =$ 20 nm is also possible, but the *s*-polarized spectrum and *p*-polarized spectrum should be measured separately, and a high dynamic range detector should be used. Finally, we design an optical test structure with the thickness of organic layer $h_0 = 160$ nm, in which three orientation parameters could be measured precisely.

Non-polarized spectra with different orientation parameters, when the thickness of the organic layer is 160 nm, are shown in Fig. 5. These simulated results show that the orientation parameters proposed in our theory do cause significant difference on the spectra and could be used for extracting orientation parameters from the spectra. Here, we further explain these differences of each orientation parameter from the perspective of the dipole radiation pattern, showing the consistence with our dipole orientation theory. For an electric dipole, it hardly radiates along the direction of its dipole vector, as the orientation of the dipole vector tends to be parallel to the z axis (v_z increases), and its intensity along the z axis 0 deg emission angle becomes weak. Thus, the normalized non-polarized spectra have stronger intensities at large emission angles, as illustrated in Fig. 5 (red lines). When the orientation of the dipole vector is parallel to the x axis (v_x increases), the normalized non-polarized spectra have weaker intensities at large emission angles, shown in Fig. 5 (yellow lines). When the total internal reflection occurs at the interface between the air layer and the emitting layer, the distribution parameter $v_{x,z}$, describing the coupling effect, has no

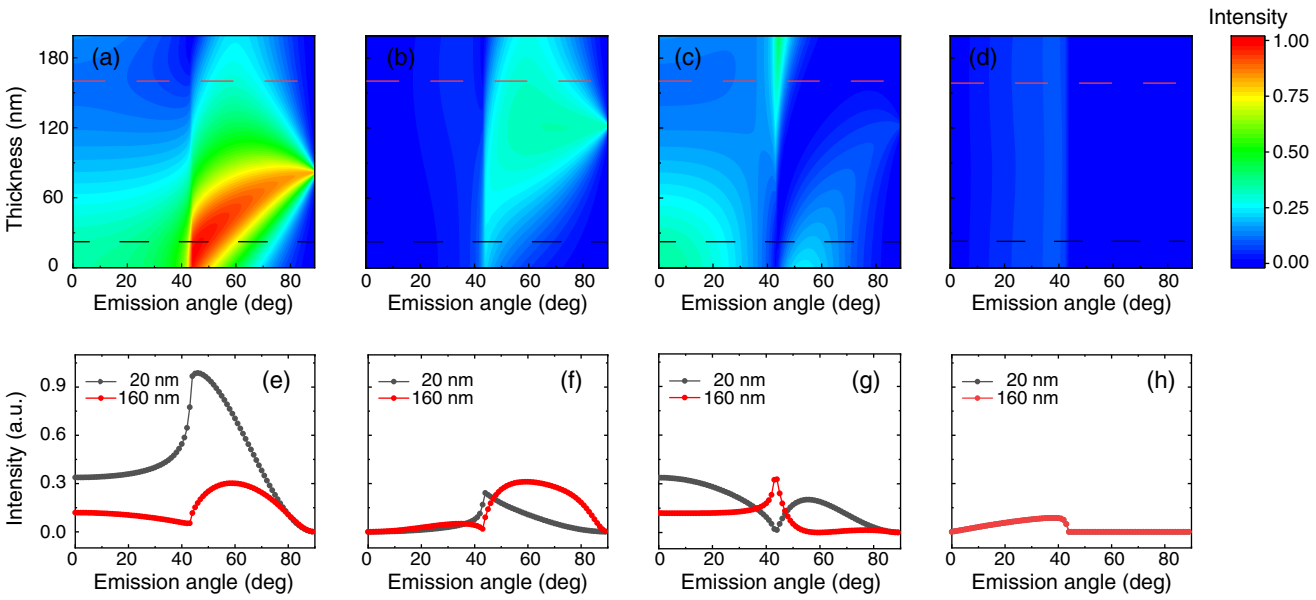

Fig. 4. Determining thickness h_0 of the test structure for extracting orientation parameters v_x, v_z, and $v_{x,z}$. (a)–(d) Simulated different components of the power densities $\widetilde{\mathcal{P}}^{s}_{\pm}$, $\widetilde{\mathcal{P}}^{p1}_{\pm}$, $\widetilde{\mathcal{P}}^{p2}_{\pm}$, and $-\widetilde{\mathcal{P}}^{p3}_{\pm}$ at different emission angles and different thicknesses. (e)–(h) Different components of the power density at different emission angles with thickness $h_0 = 20$ nm (black line) and $h_0 = 160$ nm (red line).

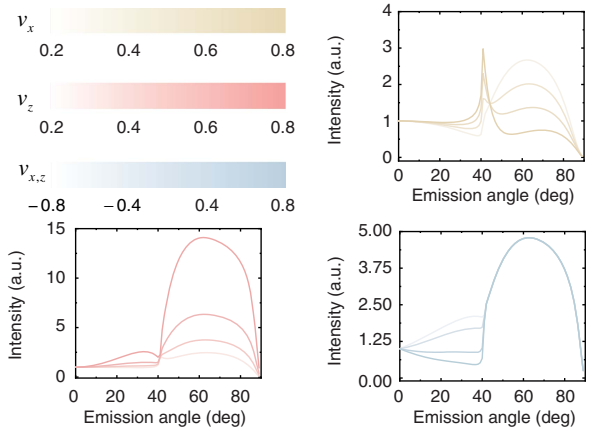

Fig. 5. Simulated spectra with different orientation parameters and thickness h_0 of the test structure at 160 nm. Simulated spectra with different parameters v_z (red lines), $v_x = 0.5$, and $v_{x,z} = 0$. Simulated spectra with different parameters v_x (yellow lines), $v_z = 0$, and $v_{x,z} = 0$. Simulated spectra with different parameters $v_{x,z}$ (blue lines), $v_z = 0.5$, and $v_x = 0.5$.

effect on the power density, as shown in Eq. (12). The distribution parameter $v_{x,z}$ only affects intensities where the emission angle is smaller than the total internal reflection angle, as illustrated in Fig. 5 (blue lines).

3.3. Parameter retrieval

We simulated radiation of 1000 dipoles with different orientations in the test structure ($h_0 = 160$ nm), obtained their radiation spectrum, and calculated their four Fourier components and orientation parameters, as shown in Fig. 6(a). Then, Gaussian noise is added into the radiation spectrum to imitate the experimental noise in reality. We retrieve the parameters from the radiation spectra, whose orientation parameters are already known as ground truth to validate the parameter extraction of our theory. In the retrieval process, random orientation parameters are chosen as an initial guess, as shown in Fig. 6(b) (gray line). The least squares algorithm (Levenberg–Marquardt algorithm) is used for fitting and extracting. The final fitting

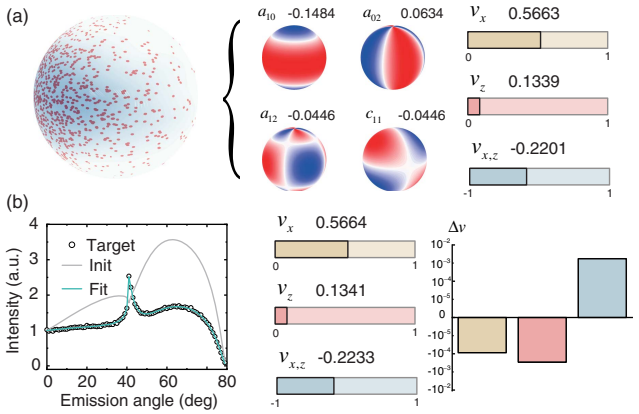

Fig. 6. Results of orientation parameter retrieval. (a) Orientation distribution of 1000 simulated dipoles, which has a Gaussian distribution centered at $\theta = 80°$ and $\phi = 200°$ (left). The four Fourier components of this distribution (middle). The calculated orientation parameters by Eq. [16] (right). (b) The target, initial, and fitting spectra (left). Extracted orientation parameters from the target spectrum (middle). The difference between the real and extracted orientation parameters (right).

spectrum is in good agreement with the target spectrum, as shown in Fig. 6(b) (green line). Also, the retrieved orientation parameters are consistent with orientation parameters of the simulated dipole orientation distribution. All of the trials show the capability of extracting the three orientation parameters from non-polarized spectra and the experimental feasibility.

4. Conclusions

By introducing an orientation distribution function to extend the power density of a dipole to the power density of the dipoles in OLEDs, it is the first time, to the best of our knowledge, to strictly prove that only three orientation parameters are needed to fully describe the relationship between the dipole orientations and the power density. These three orientation parameters could adjust the ratio of different components of the power density. Therefore, the orientation parameter can be extracted from the power density of the dipoles in OLEDs.

We design a test structure with the thickness of organic layer $h_0 = 160$ nm for extracting the three orientation parameters. Then, we retrieve the orientation parameters from the non-polarized spectrum to verify the capability and experimental feasibility. With the improvement of OLED manufacturing technology, more precise control of the dipole orientations in OLEDs is required. Our method, fully describing the dipole orientations in OLEDs, thereby provides guidance for OLED manufacturing technology.

Acknowledgement

We thank Xiaoyuan Hou, Shaobo Liu, and Zhenghong Li for fruitful discussions. This work was supported by the China National Key Basic Research Program (No. 2018YFA0306201) and the National Natural Science Foundation of China (Nos. 11774063, 11727811, and 91963212). L.S. was further supported by the Science and Technology Commission of Shanghai Municipality (Nos. 19XD143600, 2019SHZDZX01, 19DZ2253000, 20501110500, and 21DZ1101500). H.Y. has financial interest in Ideaoptics Instruments Co., Ltd. The remaining authors declare that they have no conflicts of interest. The data that support the findings of this study are available from the corresponding author upon reasonable request.

References

1. C. W. Tang and S. A. VanSlyke, "Organic electroluminescent diodes," Appl. Phys. Lett. **51**, 913 (1987).
2. H. Nakanotani, T. Higuchi, T. Furukawa, K. Masui, K. Morimoto, M. Numata, H. Tanaka, Y. Sagara, T. Yasuda, and C. Adachi, "High-efficiency organic light-emitting diodes with fluorescent emitters," Nat. Commun. **5**, 4016 (2014).
3. Y.-H. Kim, H.-C. Jeong, S.-H. Kim, K. Yang, and S.-K. Kwon, "High-purity-blue and high-efficiency electroluminescent devices based on anthracene," Adv. Funct. Mater. **15**, 1799 (2005).
4. D. H. Kim, A. D'Aléo, X. K. Chen, A. Sandanayaka, D. Yao, L. Zhao, T. Komino, E. Zaborova, G. Canard, and Y. Tsuchiya, "High-efficiency electroluminescence and amplified spontaneous emission from a thermally activated delayed fluorescent near-infrared emitter," Nat. Photonics **12**, 98 (2018).
5. M. A. Baldo, D. F. O'Brien, Y. You, A. Shoustikov, S. Sibley, M. E. Thompson, and S. R. Forrest, "Highly efficient phosphorescent emission from organic electroluminescent devices," Nature **395**, 151 (1998).
6. M. A. Baldo, S. Lamansky, P. E. Burrows, M. E. Thompson, and S. R. Forrest, "Very high-efficiency green organic light-emitting devices based on electrophosphorescence," Appl. Phys. Lett. **75**, 4 (1999).
7. M. G. Helander, Z. B. Wang, J. Qiu, M. T. Greiner, D. P. Puzzo, Z. W. Liu, and Z. H. Lu, "Chlorinated indium tin oxide electrodes with high work function for organic device compatibility," Science **332**, 944 (2011).
8. K. H. Kim and J. J. Kim, "Origin and control of orientation of phosphorescent and TADF dyes for high-efficiency OLEDs," Adv. Mater. **30**, 1705600 (2018).
9. R. Costa, G. Fernández, L. Sánchez, N. Martín, E. Ortí, and H. Bolink, "Dumbbell-shaped dinuclear iridium complexes and their application to light-emitting electrochemical cells," Chem. Eur. J. **16**, 9855 (2010).
10. P. Ren, S. Wei, P. Zhang, and X. Chen, "Probing fluorescence quantum efficiency of single molecules in an organic matrix by monitoring lifetime change during sublimation," Chin. Opt. Lett. **20**, 073602 (2022).
11. C. L. Lin, T. Y. Cho, C. H. Chang, and C. C. Wu, "Enhancing light outcoupling of organic light-emitting devices by locating emitters around the second antinode of the reflective metal electrode," Appl. Phys. Lett. **88**, 081114 (2006).
12. M. Flämmich, M. C. Gather, N. Danz, D. Michaelis, and K. Meerholz, "*In situ* measurement of the internal luminescence quantum efficiency in organic light-emitting diodes," Appl. Phys. Lett. **95**, 263306 (2009).
13. S. Nowy, B. C. Krummacher, J. Frischeisen, N. A. Reinke, and W. Brütting, "Light extraction and optical loss mechanisms in organic light-emitting diodes: influence of the emitter quantum efficiency," J. Appl. Phys. **104**, 123109 (2008).
14. G. Chen, J. Zhu, and X. Li, "Influence of a dielectric decoupling layer on the local electric field and molecular spectroscopy in plasmonic nanocavities: a numerical study," Chin. Opt. Lett. **19**, 123001 (2021).
15. J. Frischeisen, D. Yokoyama, C. Adachi, and W. Brütting, "Determination of molecular dipole orientation in doped fluorescent organic thin films by photoluminescence measurements," Appl. Phys. Lett. **96**, 073302 (2010).
16. W. Brütting, J. Frischeisen, T. D. Schmidt, B. J. Scholz, and C. Mayr, "Device efficiency of organic light-emitting diodes: progress by improved light outcoupling," Phys. Status Solidi A **210**, 44 (2013).
17. M. Flämmich, S. Roth, N. Danz, D. Michaelis, A. H. Bräuer, M. C. Gather, and K. Meerholz, "Measuring the dipole orientation in OLEDs," Proc. SPIE **7722**, 77220D (2010).
18. T. Lampe, T. D. Schmidt, M. J. Jurow, P. I. Djurovich, M. E. Thompson, and W. Brütting, "Dependence of phosphorescent emitter orientation on deposition technique in doped organic films," Chem. Mater. **28**, 712 (2016).
19. T. Komino, Y. Oki, and C. Adachi, "Dipole orientation analysis without optical simulation: application to thermally activated delayed fluorescence emitters doped in host matrix," Sci. Rep. **7**, 8405 (2017).
20. H. Cho, C. W. Joo, B.-H. Kwon, N. S. Cho, and J. Lee, "Non-linear relation between emissive dipole orientation and forward luminous efficiency of top-emitting organic light-emitting diodes," Org. Electron. **62**, 72 (2018).
21. Y. Hasegawa, Y. Yamada, M. Sasaki, T. Hosokai, H. Nakanotani, and C. Adachi, "Well-ordered 4CzIPN ((4s,6s)-2,4,5,6-tetra(9-H-carbazol-9-yl) isophthalonitrile) layers: molecular orientation, electronic structure, and angular distribution of photoluminescence," J. Phys. Chem. Lett. **9**, 863 (2018).
22. R. Chance, A. Prock, and R. Silbey, "Lifetime of an emitting molecule near a partially reflecting surface," J. Chem. Phys. **60**, 2744 (1974).
23. W. Lukosz and R. Kunz, "Light emission by magnetic and electric dipoles close to a plane interface. I. Total radiated power," J. Opt. Soc. Am. A **67**, 1607 (1977).
24. R. R. Chance, A. Prock, and R. Silbey, *Molecular Fluorescence and Energy Transfer Near Interfaces* (Wiley, 1978).
25. W. Lukosz, "Theory of optical-environment-dependent spontaneous-emission rates for emitters in thin layers," Phys. Rev. B **22**, 3030 (1980).
26. W. Lukosz, "Light emission by multipole sources in thin layers. I. Radiation patterns of electric and magnetic dipoles," J. Opt. Soc. Am. A **71**, 744 (1981).
27. G. Ford and W. Weber, "Electromagnetic interactions with metal surfaces," Phys. Rep. **113**, 195 (1984).

28. K. Neyts, "Simulation of light emission from thin-film microcavities," J. Opt. Soc. Am. A **15**, 962 (1998).
29. W. Barnes, "Fluorescence near interfaces: the role of photonic mode density," J. Mod. Opt. **45**, 661 (1998).
30. T. D. Schmidt, T. Lampe, M. R. D. Sylvinson, P. I. Djurovich, M. E. Thompson, and W. Brütting, "Emitter orientation as a key parameter in organic light-emitting diodes," Phys. Rev. Appl. **8**, 037001 (2017).
31. D. Yokoyama, "Molecular orientation in small-molecule organic light-emitting diodes," J. Mater. Chem. **21**, 19187 (2011).
32. L. Jiang, X. Luo, Z. Luo, D. Zhou, B. Liu, J. Huang, J. Zhang, X. Zhang, P. Xu, and G. Li, "Interface and bulk controlled perovskite nanocrystal growth for high brightness light-emitting diodes," Chin. Opt. Lett. **19**, 030001 (2021).
33. V. C. Sundar, J. Zaumseil, V. Podzorov, E. Menard, R. L. Willett, T. Someya, M. E. Gershenson, and J. A. Rogers, "Elastomeric transistor stamps: reversible probing of charge transport in organic crystals," Science **303**, 1644 (2004).
34. T. Amaya, S. Seki, T. Moriuchi, K. Nakamoto, T. Nakata, H. Sakane, A. Saeki, S. Tagawa, and T. Hirao, "Anisotropic electron transport properties in sumanene crystal," J. Am. Chem. Soc. **131**, 408 (2009).
35. K. Baek, D. M. Lee, Y. J. Lee, H. Choi, and J. H. Kim, "Simultaneous emission of orthogonal handedness in circular polarization from a single luminophore," Light Sci. Appl. **8**, 120 (2019).
36. C. C. Katsidis and D. I. Siapkas, "General transfer-matrix method for optical multilayer systems with coherent, partially coherent, and incoherent interference," Appl. Opt. **41**, 3978 (2002).
37. L. Li, "Formulation and comparison of two recursive matrix algorithms for modeling layered diffraction gratings," J. Opt. Soc. Am. A **13**, 1024 (1996).
38. L. Zhao, T. Komino, M. Inoue, J.-H. Kim, J. C. Ribierre, and C. Adachi, "Horizontal molecular orientation in solution-processed organic light-emitting diodes," Appl. Phys. Lett. **106**, 063301 (2015).
39. T. Komino, H. Tanaka, and C. Adachi, "Selectively controlled orientational order in linear-shaped thermally activated delayed fluorescent dopants," Chem. Mater. **26**, 3665 (2014).
40. C. A. Wächter, N. Danz, D. Michaelis, M. Flämmich, S. Kudaev, A. H. Bräuer, M. C. Gather, and K. Meerholz, "Intrinsic OLED emitter properties and their effect on device performance," Proc. SPIE **6910**, 691006 (2008).